Korean J. Chem. Eng., 34(9), 2471-2479 (2017)
DOI: 10.1007/s11814-017-0156-4

pISSN: 0256-1115
eISSN: 1975-7220

Selective deposition of Au-Pt alloy nanoparticles on ellipsoidal zirconium titanium oxides for reduction of 4-nitrophenol

Zewu Zhang*,,†, Jinghui Zhang**, Guangqing Liu***, Mengwei Xue***, Zhangzhong Wang*,**, Xiaohai Bu*,**, Qiong Wu*,**, and Xuejuan Zhao*,****

*Jiangsu Key Laboratory of Advanced Structural Materials and Application Technology, Nanjing 21167, P. R. China
**School of Materials Science and Engineering, Nanjing Institute of Technology, Nanjing 21167, P. R. China
***School of Environmental Science, Nanjing Xiaozhuang University, Nanjing 21171, P. R. China
(*Received 15 December 2016 • accepted 31 May 2017*)

Abstract−Au-Pt alloy nanoparticles that are selectively anchored on TiO_2 surface of the ellipsoidal zirconium titanium composite oxides were successfully prepared by a facile two-step method: prefabricated binary composite oxides on the ellipsoidal Fe_2O_3@SiO_2 by a versatile cooperative template-directed coating method, and then *in situ* formation of Au-Pt alloy NPs with Sn^{2+} as the reduction agent. The alloy catalysts were characterized by X-ray diffraction, transmission electron microscopy and X-ray photoelectron spectroscopy. The result suggested that highly dispersive and ultrafine Au-Pt alloy nanoparticles were deposited onto TiO_2 surface of the binary oxides solely. The particle size of nanoalloys was closely related to the ratio of Zr : Ti in the composite oxides shell. Increasing the content of Zr element led to a growth in the size of alloy nanoparticles. When used as catalysts for the reduction of 4-nitrophenol, the prepared supported alloyed catalysts exhibited high catalytic activity, and the sample could be easily recycled without a significant decrease of the catalytic activity.

Keywords: Au-Pt Alloy, TiO_2, ZrO_2, Magnetically Recycling, Selectively Deposition

INTRODUCTION

The ability to design and prepare hierarchical structure materials with molecular scale accuracy is of significant importance to gain new materials properties [1,2]. By rationally arranging the building blocks in hierarchical structures, one can produce novel materials with properties that are quite different from those expected from the simple sum of the individual blocks [3]. Actually, the interactions between the constituent parts in nanometer-scale ensembles usually lead to novel electronic, optical, or catalytic properties not available in the initial building blocks [4]. In particular, noble metal nanoparticles have emerged as highly beneficial building blocks for the preparation of various catalysts. For instance, composites containing Au and TiO_2 have received great attention for applications in CO oxidation [5], photodegradation [6], and selective hydrogenation [7]. Hybrids of Pt and porous inorganic materials are widely used as a high efficient catalyst for the dehydrogenation of light alkane [8]. The main advantages of using Au or Pt NPs as active sites of catalysts are their excellent activity and good selectively at a lower reaction temperature.

Coupling of Au and Pt atoms to construct Au-Pt bimetallic alloy NPs has been the subject of many studies [9-12]. In this nanostructure, the composite particles often exhibit distinct properties from those of their pure monometallic NP components due to the intensive interaction of the two components [13]. This strong interaction between Au and Pt may give rise to an increased performance in many heterogeneous catalysis [14]. It has been suggested that the catalytic activity is closely related to the properties of Au-Pt alloy NPs. Slight changes in their structure, size and chemical compositions can significantly influence their catalytic properties [15,16]. Generally, the tiny NPs with ultrafine size can increase the surface area, the number of edges and corner atoms, which may greatly improve their catalytic properties [17-19]. Hence, it is interesting to prepare the Au-Pt bimetallic alloy NPs as small as possible to increase the accessible surface atoms. However, the surface energy of noble metal NPs increases with the reduction of the particle size, leading to the NPs unstable with promoting particle aggregation [20]. To avoid the aggregation, various stabilizers such as polymers [21], dendrimers [22], amino or thiol ligands [23,24] have been used as capping agents to stabilize NPs. However, these organic stabilizers have obvious disadvantages for the application of the catalysts. On one hand, the presence of these capping agents around the NPs may limit their contact with reactant. On the other hand, the pretreatment of catalysts (usually roasting at high temperature) will severely destroy the organic stabilizers. In that case, the aggregation of NPs should very easily occur and thus lose their activity. Very recently, tin species have emerged as highly beneficial inorganic ligands that can protect noble metal NPs from aggregation [25]. As the inorganic ligands possess high thermal stability, linkage of NPs with tin species may be a promising strategy to increase the stability of NPs.

Another promising aspect to increase the performance of bimetallic nanocatalysts is the use of suitable support. A previous study of noble metal catalysts suggested that the support may not only

†To whom correspondence should be addressed.
E-mail: seuzzw06@163.com

serve as physical barrier that isolates the formed NPs on their surface [26], but also participates in some catalysis for their strong synergistic effect with noble metal NPs, especially for some metal oxides, such as CeO_2, TiO_2 and Fe_2O_3 [27-29]. The supports of the commercial catalysts, no matter whether natural or synthetic, usually contain more than one component. The interaction between each component may endow the support with favorable surrounding acid/base and redox sites or desired metal/metal oxide interfaces, and thus extend the application and increase the activity of the supported noble metal NPs. Nonetheless, the interaction between noble metal NPs and support varies with the oxides. In this regard, the preparation of Au-Pt alloy NPs that support on binary or ternary metallic oxides may be more meaningful.

ZrO_2, TiO_2 and their binary composites have been widely employed in various fields including catalysis, heavy metal ion waste sequestration and dye-sensitized solar cells [30,31]. Compared to the individual ZrO_2 or TiO_2, the ZrO_2-TiO_2 binary oxide shows improved stability since the presence of -Zr-O-Ti-O-Zr- networks can retard the crystallization of the individual components, leading to an amorphous binary metal oxide framework with high surface area and adjustable porosity [32,33]. Moreover, such ZrO_2-TiO_2 mixed oxides also exhibit modifiable surface properties, which could promote the applicability of the binary oxide as a high performance catalyst. As a reducible metallic oxide, TiO_2 possesses a much stronger synergistic effect with noble metal NPs than ZrO_2 [34]. Therefore, selective anchoring of noble metallic NPs on TiO_2 instead of ZrO_2 may allow the maximum interaction among each composite and give an improved catalytic activity. Until now, however, there have been few reported examples of directional incorporation of noble metal NPs on the composites support. It remains a great challenge to develop general and effective strategies for preparing these supported Au-Pt alloy NPs selective anchored on TiO_2 surface that existed in the ZrO_2-TiO_2 composited supports.

Additionally, magnetic separation provides a convenient method for removing and recycling magnetized species by applying an outside magnetic field. This approach may prevent the agglomeration of the catalyst particles during recovery and can increase the durability of the catalysts. In this regard, it seems to be more meaningful to incorporate a magnetized core into the catalytic system.

Herein, we report a versatile *in situ* reduction method to prepare Au-Pt nanocatalyst that selectively supported on ZrO_2-TiO_2 mixed oxides. In the first step, the ellipsoidal Fe_2O_3@SiO_2 NPs were coated with a uniform layer of ZrO_2-TiO_2 binary oxide via sol-gel method using HDA as the soft template. Then, the obtained matrices were activated in a $SnCl_2$ solution by the inorganic grafting between Sn^{2+} and hydroxyl group on the support. As the sol-gel derived binary oxides have abundant hydroxyl group on TiO_2 surface while little on ZrO_2 surface [35], it is proposed that the Sn^{2+} was mainly linked on TiO_2 surface. Then the tiny Au-Pt alloyed NPs with well-dispersed distribution were assembled on the TiO_2 surface via the *in situ* reduction by Sn^{2+}. Lastly, the obtained Fe_2O_3@ZrO_2-TiO_2/Au-Pt suffered from a calcination and subsequent reduction process, in which process the non-magnetic Fe_2O_3 core could be transformed to Fe core with high saturation magnetization and endowed the composites with excellent magnetic separation properties. It was found that the particles size of nanoalloys was closely related to the ratio of Zr : Ti in the composite oxides shell. Increasing the content of Zr element led to a growth in the size of alloy nanoparticles. The prepared Fe@ZrO_2-TiO_2/Au-Pt hybrid NPs exhibited a high activity and good reusability as catalysts for the reduction of 4-nitrophenol to 4-aminophenol.

EXPERIMENT

1. Materials

Gold(III) chloride trihydrate ($HAuCl_4 \cdot 3H_2O$, ≥99.9%), potassium tetrachoroplatinate (K_2PtCl_4, ≥96%), tetrabutyl titanate (TBOT, 95%), zirconium(IV) n-butoxide solution (80 wt% in butanol, $Zr(n\text{-}Bu)_4$ for short), 1-hexadecylamine (HDA) and 4-nitrophenol (≥99%) were purchased from Aldrich. $FeCl_3$, KH_2PO_4, tetraethyl orthosilicate (TEOS), isopropanol, ethanol, ammonia (25 wt%) and $SnCl_2 \cdot 2H_2O$ were of analytical grade, and all of them were purchased from Sinopharm Chemical Reagent Co., Ltd. Deionized water was used in all experiment. All chemicals were used as received without further purification.

2. Synthesis of Fe_2O_3@ZrO_2-TiO_2

Monodispersed Fe_2O_3@SiO_2 NPs with an ellipsoidal Fe_2O_3 core and a thin SiO_2 layer were obtained according to the previous reported method [36]. The purified Fe_2O_3@SiO_2 NPs were dispersed in ethanol to form a colloidal solution with the concentration about 2 mg/mL. Then 50 mL of the colloidal solution was added into a mixture solution containing ethanol (50 mL), HDA (0.25 g), and ammonia (0.5 mL) with mechanical stirring. Then 0.4 mL of mixed solution of $Zr(n\text{-}Bu)_4$ and TBOT that dissolved in ethanol (25 mL) was slowly added to the colloidal mixture. After injection, the solution was kept to stir for 4 h, and then aged for 12 h. The Fe_2O_3@ZrO_2-TiO_2 matrices were separated from solution by centrifugation and washed with ethanol. The samples were termed Fe_2O_3@ZrO_2-TiO_2 (x : y), where x : y stands for the nominal ratio of ZrO_2 : TiO_2 in the binary oxides shell.

3. Synthesis of Fe_2O_3@ZrO_2-TiO_2/Au-Pt Nanocapsules

The *in situ* formation of Au-Pt bimetallic NPs were prepared followed by the Sn^{2+} reduction method. Typically, 50 mL of the as-prepared Fe_2O_3@ZrO_2-TiO_2 solution (0.2 wt% in water) was dispersed into a mixture solution containing 100 mg of $SnCl_2 \cdot 2H_2O$ and 60 mL of 10 mM HCl. After stirring for 12 h, the precipitate was separated by centrifugation, washed with water for four times and redispersed into 30 mL water, followed by adding 66.7 μL of 0.75 wt% K_2PtCl_4 solution at room temperature and stirring for 15 min. Then, 50 μL of 1 wt% $HAuCl_4$ solution was added. After stirring for 30 min, 10 mL of 0.15 M sodium formate solution was added. After reaction for 12 h, the product was collected by centrifugation, washed with water and dried in a vacuum oven.

4. Preparation of Fe@SiO_2@ZrO_2-TiO_2/Au-Pt Nanocapsules

To completely transform Fe_2O_3@ZrO_2-TiO_2/Au-Pt nanocapsules into the magnetic Fe@ZrO_2-TiO_2/Au-Pt nanocapsules, the samples were first calcined at 550 °C for 4 h. Then, the powder was transferred to a tube furnace with ultrapure hydrogen (99.99%) flow at 525 °C for 4 h.

5. Catalytic Reaction of Reduction of 4-NP

The catalytic performance of the catalysts was checked using the reduction of 4-NP to 4-AP with $NaBH_4$ aqueous solution at

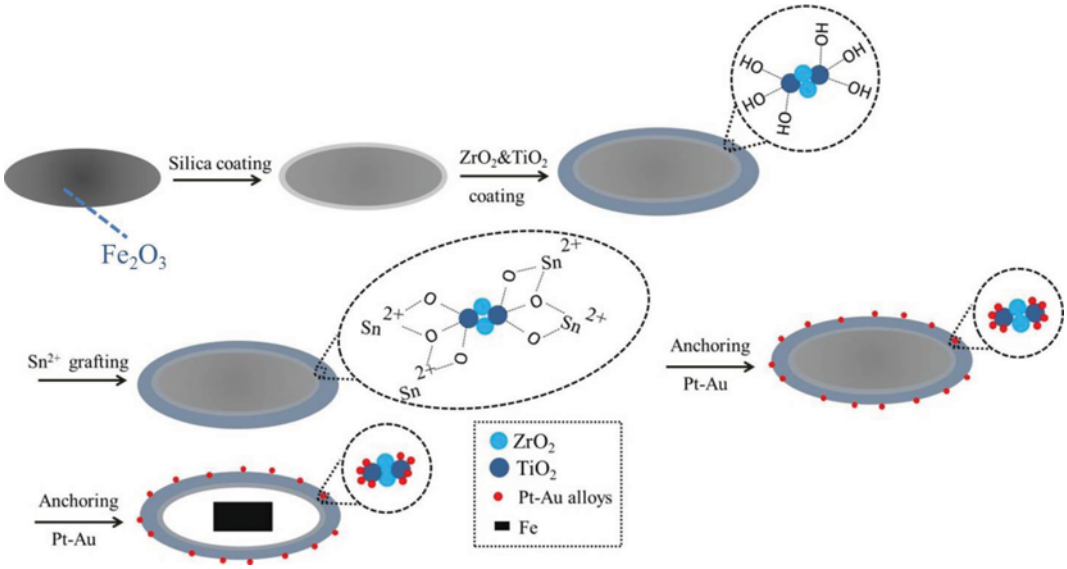

Scheme 1. The synthetic procedure for the multifunctional Fe@SiO_2/ZrO_2-TiO_2/Au-Pt hybrid catalysts.

room temperature. Typically, 0.2 mL of aqueous solution of 4-NP (0.005 M), 2 mL of aqueous solution of a fresh $NaBH_4$ (0.2 M) was added into a quartz cuvette, and then adding 0.25 mL of aqueous solution of Fe@ZrO_2-TiO_2/Au-Pt nanocapsules (0.5 mg/mL). The change of the mixture solution color was monitored using UV-vis spectroscopy.

6. Characterization

Transmission electron microscopy (TEM) experiments were conducted on a JEM-1230 microscope operated at 100 kV. The samples for the TEM measurements were suspended in ethanol and supported onto a Cu grid. Field emission scanning electron microscopy (FESEM) images and the distribution of element were carried out on a scanning electron microscope (Zeiss, Ultra Plus) unit with a high-angle annular dark-field (HAADF) detector (HITACHI S-5500) operating at 20 kV. The powder X-ray diffraction (XRD) patterns were recorded on a Bruker D8 Advance Diffractometer (Germany) with Cu Kα radiation (λ=1.5406 Å). X-ray photoelectron spectra (XPS) measurements were carried out in a Thermo ESCALAB 250 instruments (USA) using non-monochromatic Al Kα1486.6 radiation. All samples were reduced in situ under hydrogen at 500 °C for 1 h, and the spectra were recorded at room temperature in a vacuum better than 5×10^{-9} mbar. The magnetic behavior was investigated using a vibrating sample magnetometer (VSM, Lake Shore 7304, Lake Shore, USA) with an applied field between −15 kOe and 15 kOe at room temperature. UV-vis spectra were recorded on a Shimadzu UV 3600 spectrometer.

RESULTS AND DISCUSSION

1. Fabrication of Multifunctional Fe@SiO_2/ZrO_2-TiO_2/Au-Pt Hybrid Catalysts

The work aims to selectively anchor noble metal NPs on binary metallic oxides by taking the advantages of different chemical property of individual metallic oxides. The essential idea is that sol-gel derived ZrO_2-TiO_2 binary metallic oxides contain abundant hydroxyl on TiO_2 surface while little hydroxyl on ZrO_2 surface. These hydroxyl groups can serve as the active sites for loading of Sn^{2+} species and homogeneously anchoring noble metal NPs on TiO_2 surface eventually. In considering that the dualistic noble metallic catalysts may exhibit increased catalytic activity than monometal counterparts, the Pt-Au bimetal NPs were chosen as the noble metal NPs to study the selective anchor properties. But similar results can also be obtained for the monometal NPs. Additionally, to bestow the catalyst with excellent magnetically recycling, an inner magnetite Fe core material was incorporated into the binary metallic oxides.

The overall synthesis procedure for the hybrid catalysts involves five steps as depicted in Scheme 1. First, the water dispersible non-magnetite Fe_2O_3 particles were coated by a thin protecting layer of the silica, forming core-shell Fe_2O_3@SiO_2 ellipsoidal nanocomposite. Second, the resultant Fe_2O_3@SiO_2 was further coated by a layer of ZrO_2-TiO_2 composite via a convenient sol-gel coating process. Third, the sandwich structure composite was modified with Sn^{2+} species by the inorganic grafting of Sn^{2+} with hydroxyl group on TiO_2 surface. Then, the Pt-Au alloy NPs with specific distribution were assembled on the surface of the ellipsoidal NPs by taking advantage of reduction of Sn^{2+} to *in situ* formation of Au and Pt atoms. In the last step, the obtained samples suffered from a calcination and subsequent reduction process to transform the non-magnetic Fe_2O_3 core to Fe core with high saturation magnetization.

The ellipsoidal Fe_2O_3 particles were prepared through a well-established hydrothermal reaction based on high temperature hydrolysis of $FeCl_3$ in the presence of KH_2PO_4 as a stabilizer [37]. The obtained Fe_2O_3 particles had a mean length of ~350 nm and aspect ratio of ~4 (Fig. S1(a)). The particles with high aspect ratio were suggested to be favorable for obtaining the catalyst with higher activity towards some heterogeneous catalysis [38]. These ellipsoidal particles were then coated with a thin silica shell via the hydrolysis and condensation of TEOS in according to the well-known Stöber approach. The silica coating helps to improve the dispers-

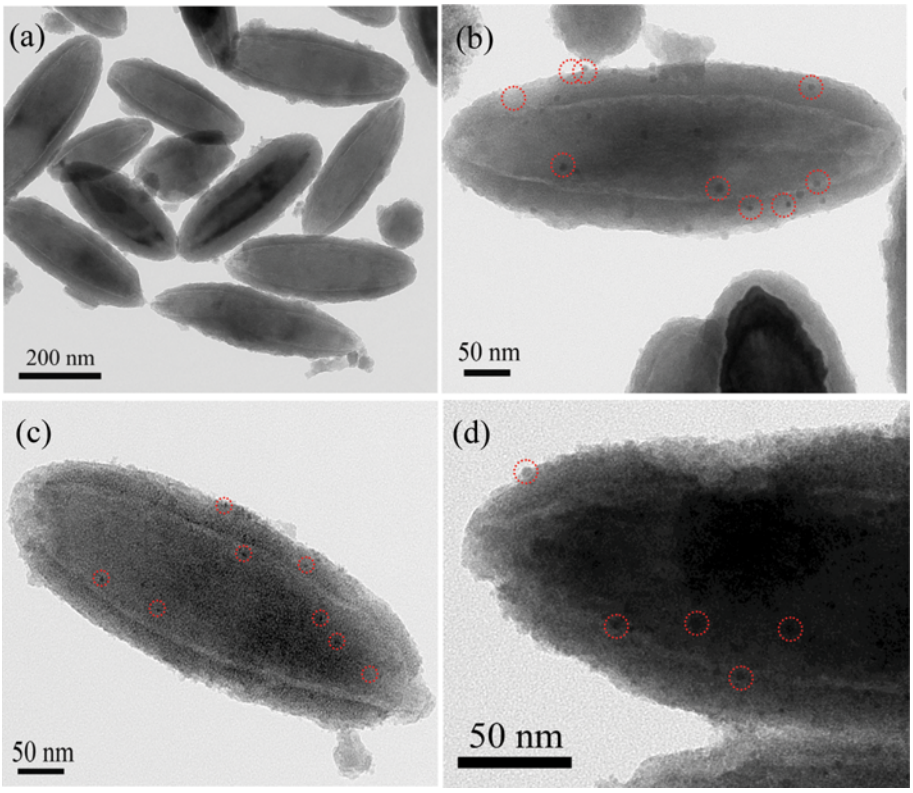

Fig. 1. (a) A representative TEM image of Fe_2O_3@ZrO_2-TiO_2 NPs (ZrO_2 : TiO_2=3 : 1) showing the uniform binary metallic oxides shell. (b)-(d) TEM images of as-prepared Fe_2O_3@ZrO_2-TiO_2(x : y)/Au-PtNPs. The x : y is (b) 3 : 1, (c) 1 : 1, and (d) 1 : 3.

ibility of the ellipsoidal particles and in hence facilitating the subsequent formation of uniform depositing. After that, a thick binary metallic oxides (ZrO_2-TiO_2) layer was formed on Fe_2O_3@SiO_2 surface through a surfactant-templated sol-gel coating process using HAD as the template and Zr(n-Bu)$_4$ and TBOT as the ZrO_2 and TiO_2 precursor, respectively. Fig. 1(a) shows a representative TEM image of the Fe_2O_3@ZrO_2-TiO_2 hybrid NPs. The image indicated that the hybrid NPs exhibited a well-defined sandwich structure with ZrO_2-TiO_2 composite layers of ~30 nm in thickness. As the hydroxyl group on composite oxides layers has a significant influence on the succeeding distribution of Sn^{2+} and Au-Pt NPs, it seems important to study the circumstance of surface hydroxyl group. In this work, pure metal oxides (ZrO_2 or TiO_2) were prepared and their surface hydroxyl group was studied by FT-IR test, respectively. As shown in Fig. S1(b), both TiO_2 and ZrO_2 samples exhibited a broad peak around 3,430 cm^{-1}, which could be attributed to the stretching vibration band of -OH from the absorbed H_2O. It was expected that the pure TiO_2 sample had abundant surface hydroxyl groups as evidenced by the presence of an additional strong peaks at ~3,760 cm^{-1}. To the contrary, the missing of the peaks of ZrO_2 sample indicated that few hydroxyl groups were located on pure ZrO_2 surface. Based on the FT-IR date, it seemed to be reasonable to deem that the ZrO_2-TiO_2 composite layers had a distinct distribution of hydroxyl, with hydroxyl-group-rich on TiO_2 while hydroxyl-group-barren on ZrO_2.

The aforementioned surface hydroxyl groups then served as the grafting site for selectively attaching Sn^{2+} on the composite oxides surface. To verify the unitary linking of Sn^{2+} on TiO_2 surface, the TiO_2 and ZrO_2 samples were first impregnated into $SnCl_2$ solution, and washed with water twice to remove the physically absorbed Sn^{2+}. The EDX analysis of the Sn^{2+} treated samples suggested that the amount of Sn species grafted on TiO_2 was ~five-fold as compared to that on ZrO_2 sample, which indirectly indicated that the Sn^{2+} might be linked on TiO_2 surface of ZrO_2-TiO_2 composite layers solely and also confirmed the distinct distribution hydroxyl groups. Afterwards, Au-Pt bimetallic NPs were *in situ* assembled on the surface of sandwich hybridized NPs. In this process, K_2PtCl_4 and $HAuCl_4$ were added successively to the aqueous solution of the above Sn^{2+} activated NPs. The linked Sn^{2+} species acted as a reducing reagent to reduce Pt^{2+} *in situ* on the surface of Fe_2O_3@ZrO_2-TiO_2 NPs, then Au^{3+} could be easily reduced by the replacement between $AuCl_4^-$ and Pt nanocrystals on supports as described previously [36,39]. Due to the unique orientation of Sn^{2+} species, the obtained Au-Pt particles were believed to be deposited on TiO_2 surface rather than on ZrO_2 surface solely.

Fig. 1(b) shows representative TEM images of the Fe_2O_3@ZrO_2-TiO_2/Au-Pt composites with the nominal ZrO_2 : TiO_2 ratio is 3 : 1. Obviously, the metal NPs were relatively uniform, possibly because TiO_2 was evenly distributed in the ZrO_2-TiO_2 composite (see later). Interestingly, the particle size of the Au-Pt bimetallic NPs varied with the ratio of Zr and Ti in the support (Fig. 1(b)-1(d)). When the ratio of ZrO_2 : TiO_2 was 3 : 1 in the binary metallic oxides, the average size of the formed Au-Pt NPs was ~7.7 nm. Whereas, the ratio of Zr : Ti was lowered to 1 : 1, Au-Pt NPs decreased to ~3 nm,

suggesting that increasing the content of Ti species in the shell can decrease the size of Au-Pt NPs significantly. Further increasing TiO_2 content in the oxides shell to 75% (Zr : Ti=1 : 3), the Au-Pt NPs had the smallest particles size with about 2.7 nm. As described above, the sol-gel derived TiO_2 incorporated rich hydroxyl groups on their surface, while the ZrO_2 surface contained fewer hydroxyl groups, thus Sn^{2+} preferred to link on TiO_2 surface. Increasing the content of TiO_2 in the shell would lead to more Sn^{2+} species on the surface, resulting in the growing density of the active sites for immobilization and reduction, and ultimately giving rise to the small size of Au-Pt NPs. The energy dispersive X-ray (EDX) spectroscopy (Fig. S3) revealed that the atomic ratio of Au and Pt in all the samples was 1.18 : 1-1.25 : 1, which was approximate to the stoichiometric proportion of initial reactants and matched well with the analysis of ~1.12 : 1 from inductively coupled plasma-mass spectrometry (ICP-MS). The actual composition of the ZrO_2-TiO_2 composite oxides shells is also given in Fig. S3, and the result suggests that the ratio of ZrO_2 : TiO_2 in the final samples depended on the samples but was close to the nominal ratio. Additionally, SEM image of the as-obtained sample (Fig. S2) shows the clearly ellipsoidal structure, suggesting the deposition of Au-Pt NPs on the support had little influence on the structure of samples. Moreover, with the aim to study the elemental distribution of Fe_2O_3@ZrO_2-TiO_2(3 : 1)/Au-Pt NPs, high-angle annular dark field scanning transmission electron microscopy (HAADF-STEM) was performed. As shown in Fig. S4, the Zr and Ti were evenly covered on the Fe_2O_3 surface. Comparing the mapping images of the Zr(Zr-K) and Ti(Ti-K), it may be concluded that ZrO_2 species were tightly bound to TiO_2 species and the shell of the sample consisted of ZrO_2-TiO_2 composite. Furthermore, the Au and Pt were also highly dispersed on the composite surface. Considering the similar distribution of Au and Pt species, the Au and Pt might on their alloyed structure.

HRTEM analysis was used to explore the possible structure of Au-Pt NPs. Fig. 2(b) shows a representative HRTEM image of the Au-Pt NPs supported on Fe_2O_3@ZrO_2-TiO_2(3 : 1), clearly displaying the abundant distribution of Au-Pt on the composite oxides. The estimated lattice spacing of 0.23 nm could be assigned to the (111) planes of Au-Pt bimetallic nanocrystals, which was slightly lower than that for the (111) lattice spacing of pure Au (0.235 nm), but larger than that expected for pure Pt (0.227 nm), suggesting the possible formation of Au-Pt alloy composition on the surface of support.

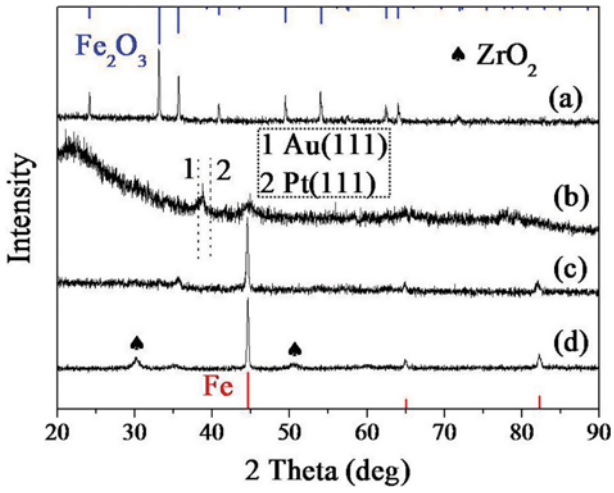

Fig. 3. XRD patterns of (a) as-prepared Fe_2O_3@SiO_2@ZrO_2-TiO_2/Au-Pt(1 : 1) NPs, and the samples after sequentially roasting at 550 °C under air and 525 °C under H_2 atmosphere: (b) SiO_2/Au-Pt NPs, (c) Fe_2O_3@SiO_2@ZrO_2-TiO_2/Au-Pt(1 : 1) NPs, and (d) Fe_2O_3@ZrO_2/Au-Pt NPs.

The crystal structure and composition of the samples were characterized by powder X-ray diffraction (XRD). Fig. 3(a) presents the XRD pattern of Fe_2O_3 @ZrO_2-TiO_2(1 : 1)/Au-Pt NPs samples. Only the characteristic diffraction peaks corresponding to α-Fe_2O_3 could be observed. No obvious peaks of ZrO_2-TiO_2 and Au&Pt in the pattern indicated amorphous characteristic of the sol-gel derived composite oxides and the relatively low amounts and high dispersion of noble metal on the support, respectively.

The thermal stability of the supported Au-Pt bimetallic NPs was tested in this study. Unlike the conventional calcination treatment, the samples suffered from sequential roasting under air and H_2 atmosphere, which may be much closer to the pretreatment and practical application of catalyst, especially for some reduction reaction. Fig. 4 displays the TEM images of the obtained samples. After the roasting treatment, the particle size of Au-Pt alloy NPs increased to about 8.4 nm, which was smaller as compared to that of Au-Pt NPs supported on SiO_2 in our previous work [36], strongly de-

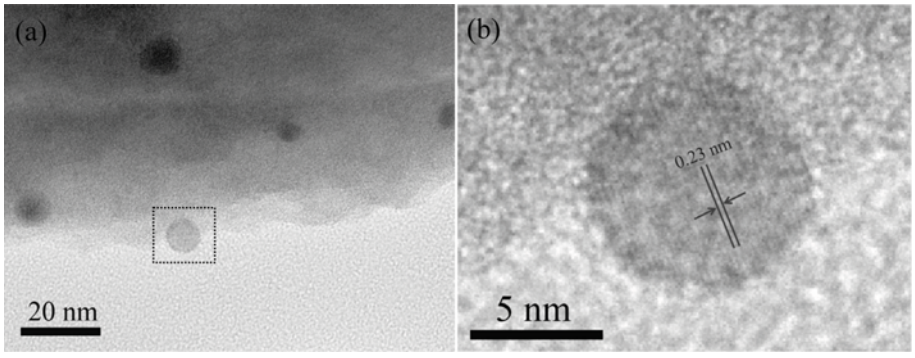

Fig. 2. (a) HRTEM image of Fe_2O_3@ZrO_2 : TiO_2(1 : 1)/Au-Pt NPs, (b) lattice fringe of Au-Pt nanoalloys is the magnified image of the interface enclosed by the black rectangular area in a.

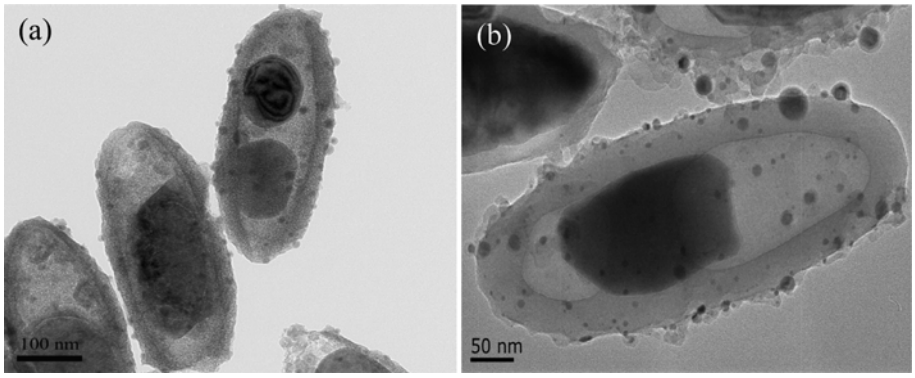

Fig. 4. The representative TEM images of (a) Fe@SiO_2@ZrO_2-TiO_2(1 :1)/Au-Pt NPs and (b) Fe@SiO_2/Au-Pt NPs.

monstrating the good thermal stability of Au-Pt NPs when incorporated with the ZrO_2-TiO_2 composite oxides. Additionally, the TEM images of the samples with ZrO_2 : TiO_2=1 : 3 were also studied and the result also indicated that the good thermal stability of Au-Pt NPs as the evidenced by the Au-Pt alloy NPs only grew to about 7.8 nm (seen in Fig. S5). Interestingly, the ellipsoidal Fe_2O_3 core was transformed into irregular core after roasting treatment, accompanied with a cavity between core and shell. Note that roasting the sample under H_2 could effectively transform the Fe_2O_3 core to magnetism Fe core, as confirmed by the disappearance of the characteristic diffraction peaks corresponding to α-Fe_2O_3 and the appearance of the Fe peaks in Fig. 3(c), which may improve the recycling performance of the catalyst used in liquid-phase reactions. Additionally, the composite oxides shell maintained their amorphous nature even after calcination and reduction, suggesting a relatively high thermal stability of the resulting amorphous sphere. In sharp contrast, the sample obtained by treating the Fe_2O_3@ZrO_2/Au-Pt NPs in the same process gave rise to more intensive characteristic peaks of the metal oxides, indicating that the binary oxides can retard the crystallization of the individual components. The low crystallinity may suppress the possible structural reforming when crystallization, therefore increasing the thermal stability of Au-Pt NPs. Additionally, the reserved amorphous binary oxides further confirmed that the Zr and Ti species were well distributed within the shells and that prevented the formation of sufficient size domains of Zr species and crystallization during calcination. To further ascertain the alloy structure of Au-Pt NPs, a twice dosage of $AuCl_4^-$ and $PtCl_4^{2-}$ was used as the prosperous and the Au-Pt alloy NPs was deposited to the SiO_2 beads directly. The XRD patterns of the obtained sample showed a prominent(111) peak at 38.8°, which was also located in between the Au(111) peak at 38.19° and Pt(111) peak at 39.81°, demonstrating the alloy struc-

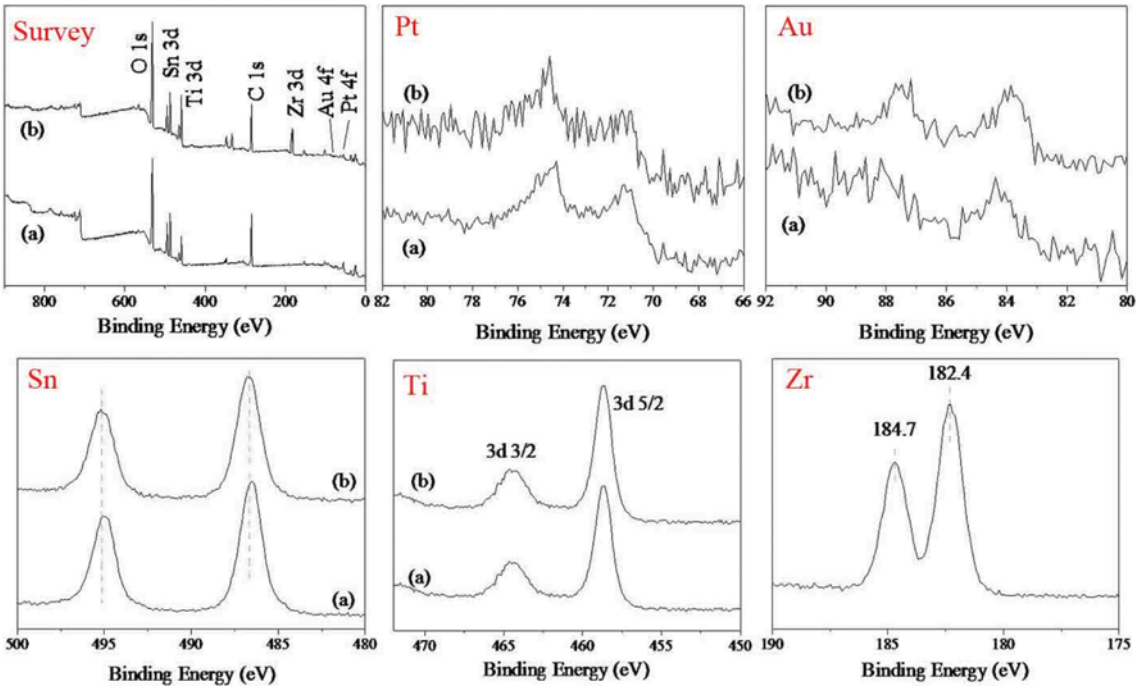

Fig. 5. XPS spectra of the (a) Fe@TiO_2/Au-Pt NPs and (b) Fe@ZrO_2-TiO_2(1 : 1)/ Au-Pt NPs.

ture of Au-Pt supported on the composite oxides.

The surface chemical environment of the Fe@ZrO_2-TiO_2(1 : 1)/Au-Pt was obtained by XPS in comparison with Fe@TiO_2@Au-Pt sample (Fig. 5). The fully scanned spectra of the two samples in the range of 0-900 eV revealed the presence of Au, Pt, Zr, Ti, O, Sn and C elements in the Fe@ZrO_2-TiO_2(1 : 1)/Au-Pt sample and the Au, Pt, Ti, O, Sn and C in the Fe@TiO_2@Au-Pt sample. These C elements should be ascribed to the adventitious carbon contaminant, and the binding energy for C1s peak at 284.6 eV was used as the reference for calibration [40]. Two Pt 4f signals of the Fe_2O_3@ZrO_2-TiO_2(1 : 1)/Au-Pt nanocomposite were found at ~71.5 eV and ~74.6 eV, corresponding to the Pt 4f7/2 and Pt 4f5/2, respectively, implying the complete reduction of Pt^{2+} ions to Pt by the linked Sn^{2+} species [41]. These signals were relatively higher than those for metallic Pt in Fe@TiO_2@Au-Pt sample, suggesting the presence a strong interaction between Pt and composite oxides. Similar result could be found in Sn 3d signals in the Fe@ZrO_2-TiO_2@Au-Pt(1 : 1) nanocomposite, which shifted toward a higher binding energy as compared with the Fe@TiO_2@Au-Pt(1 : 1) samples, suggesting incorporation of ZrO_2 in TiO_2 shell may promote the interaction among Sn^{2+} species, TiO_2 and Au-Pt NPs in consequence. As mentioned in the XRD test, the presence of the binary oxides in the shell may retard the crystallization of the individual oxides (including TiO_2), resulting in composite oxides with small TiO_2 crystallites, which was believed to bestow the catalysts with larger amount of active interface. Thus the electron transformation among metal oxides shell, Sn species and noble metal NPs increased to a certain extent. Meanwhile, the XPS spectrum of the Au 4f peaks of Fe@ZrO_2-TiO_2(1 : 1)@Au-Pt nanocomposites displayed a slight moving to the position with lower binding energy, suggesting the increased electron density on Au surface. The result also demonstrated that the incorporation of ZrO_2 in the composite oxides shell leads to a modification of electron environment of alloy NPs. The high-resolution Ti 2p spectrum in Fe@ZrO_2-TiO_2/Au-Pt exhibited peaks located at 464.3 and 458.6 eV corresponding to Ti $2p_{1/2}$ and Ti $2p_{3/2}$, respectively, which indicated the normal state of Ti^{4+} in the binary oxide shells. Additionally, the corresponding Zr 3d spectrum showed that the binding energy for Zr 3d 5/2 and Zr 3d 3/2 was located at 182.4 and 184.7 eV, respectively, which were also identified as Zr^{4+} in the composite oxides [42].

The magnetic response of the Fe@ZrO_2-TiO_2(1 : 3)/Au-Pt NCs to an external field as a representative was studied using a VSM instrument at room temperature. As shown in Fig. S6, the sample displayed a quite narrow hysteresis loop with a low coercivity and remanence, suggesting excellent paramagnetic behavior. The saturation magnetization of the as-prepared sample was measured to be 91.9 emu/g, which is a large value for the sample to be manipulated conveniently by an external magnetic field [43,44]. As a result, on placing a magnet beside the vial, the sample was quickly attracted to the side of the vial and the solution became transparent. This characteristic provides an easy and efficient way to separate the Fe@ZrO_2-TiO_2/Au-Pt NPs from the reaction mixture for reuse under an external magnetic field.

2. Catalytic Properties of the Supported Au-Pt Nanoalloys

The catalytic properties of the Fe@ZrO_2-TiO_2/Au-Pt nanocatalysts were quantitatively evaluated with the reduction of 4-NP into 4-AP by $NaBH_4$ as a model system [9,45,46]. The reduction reaction could be monitored using the UV-Vis spectrum because 4-NP and 4-AP had different absorbance in the UV-Vis range (λ_{max}= 400 nm and 300 nm, respectively) [47-49]. The reduction reaction does not occur without the presence of Au or Pt particles as catalyst, as evidenced by little change in the absorption peak after standing for 2 h. After addition of a trace amount of catalysts into the solution, the adsorption peak significantly decreased, suggesting the reaction proceeded. Fig. 6(i) shows plots of C_t/C_0, where C_0 and C_t are the concentrations of the 4-NP at t=0 s and time t, respectively. Considering the concentration of $NaBH_4$ is much higher than 4-NP, the reaction rate can be assumed to be independent of the concentration of $NaBH_4$. Hence, pseudo-first-order rate kinetics with regard to the concentration of 4-NP can be used to evaluate the catalytic rate. The linear relationships between $\ln(C_t/C_0)$ and reaction time in the reduction reaction using the samples are shown in Fig. 6, and the plots well match the first-order reaction kinetics. The rate constant k could be calculated from the slope of the straight lines.

The calculated k was 0.06 min^{-1} and 0.77 min^{-1} for Fe@ZrO_2/Au-Pt and Fe@ZrO_2-TiO_2(3 : 1)/Au-Pt samples, respectively. The result indicated that incorporating the TiO_2 component into the metal oxides shells gave rise to significantly improved catalytic activity. It is suggested that the pure ZrO_2 shell has little deposited sites for loading Au-Pt NPs, which might lead to less content and larger particles size of noble metal. Instead, the TiO_2-ZrO_2 com-

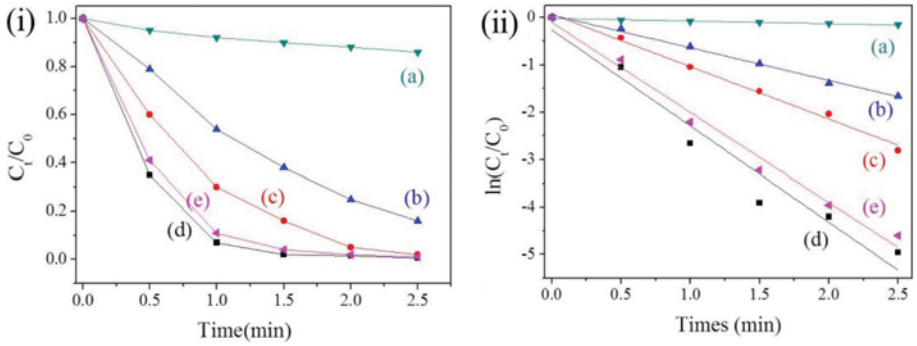

Fig. 6. (i) Variation of C_t/C_0 with time and (ii) $\ln(C_t/C_0)$ for the catalysts: (a) Fe@ZrO_2/Au-Pt, (b) Fe@ZrO_2-TiO_2(3 : 1)/Au-Pt, (c) Fe@ZrO_2-TiO_2(1 : 1)/Au-Pt, (d) Fe@ZrO_2-TiO_2(1 : 3)/Au-Pt and (e) Fe@TiO_2/Au-Pt.

posite oxides contained abundant sites for linking of Au-Pt NPs, and therefore Au-Pt component on ZrO_2-TiO_2 shells had a quite high content with small particle size. Thus, the Fe@ZrO_2-TiO_2(3 : 1)/Au-Pt samples exhibited an enhanced catalytic activity than that of Fe@ZrO_2/Au-Pt. Additionally, the catalytic activity of the Fe@ZrO_2-TiO_2/Au-Pt samples could be tuned easily by changing the ratio of ZrO_2 to TiO_2, as evidenced by the k values of Fe@ZrO_2-TiO_2(1 : 1)/Au-Pt and Fe@ZrO_2-TiO_2(1 : 3)/Au-Pt samples which were 1.78 min^{-1} and 2.67 min^{-1}, respectively. The result also suggested that increasing the percentage of TiO_2 in the binary oxides shell led to the improving in the performance of the Fe@ZrO_2-TiO_2/Au-Pt samples. The enhanced catalytic performance might be ascribed to the smaller particle size of Au-Pt NPs with the increase in the content of TiO_2. Interestingly, the Fe@ZrO_2-TiO_2(1 : 3)/Au-Pt samples even had a higher catalytic activity towards the reduction of 4-NP as compared with the pure TiO_2 counterpart (2.43 for Fe@TiO_2/Au-Pt samples). As discussed, the doping ZrO_2 into the oxides shell restricted the phase transformation of TiO_2 during the process of thermal treatment and gave rise to small crystalline particles of TiO_2, which may increase the synergistic effect among noble metal NPs, Sn species and support. Therefore, higher catalytic activity can be obtained than that for Fe@TiO_2/Au-Pt samples. Furthermore, we compared the normalized rate constant (the molar of noble metals specific activity) with that of Au-based and Pt-based nanocatalysts reported previously as listed in Table S1 in the Supporting Information. It can be found that the normalized k values of the Fe@ZrO_2-TiO_2(1 : 3)/Au-Pt samples are much higher than those of most reports for the catalytic reduction of 4-NP by $NaBH_4$.

On the basis of the above experimental results and theory analysis, a possible catalytic mechanism is illustrated in Fig. 7. According to the traditional theory on the reduction of 4-NP by noble metal NPs, the reaction was by electron transfer from BH_4^- to 4-NP on the metal NPs surface [50]. In our work, the formation of Au-Pt alloy structure could alter the electronic structure of the involved metal atoms. As reported, electronic transformation from Pt to Au was intense and easy, which may give rise to an electron-enriched region around Au surface and a positive charge-enriched region around Pt NPs simultaneously [51]. The Pt NPs surrounded with positive charge can adsorb BH_4^- easily through the electrostatic interactions, and then the absorbed BH_4^- is dissociated on Pt surface to [H^-]. These [H^-] can be then transferred to Au surface and trigger the reduction of 4-NP. The support may also have a

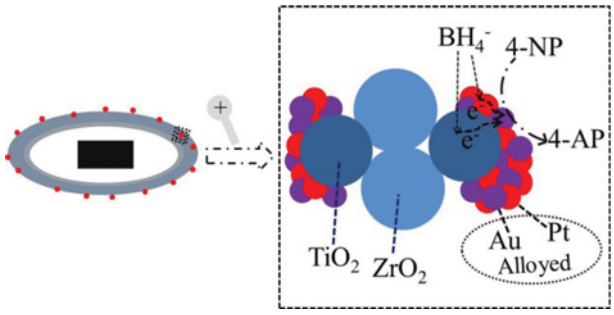

Fig. 7. A possible reaction mechanism for reduction of 4-NP on Fe@ZrO_2-TiO_2/Au-Pt.

strong influence on the catalytic performance, especially for TiO_2, which exhibits strong "support-metal" interaction. For the reduction of 4-NP, TiO_2 is also suggested to take part in the reaction. As Au (5.1 eV) has a higher work function than that of TiO_2 (3.2 eV), electrons may also tend to leave TiO_2 to the Au NPs until arriving at a comparable Fermi level [52]. The process leaves behind positively charged regions on TiO_2 surface and serves as the additional dissociative adsorption sites for oxidizing of BH_4^- to BO_2^- and releasing [H^-] to Au surface, which inevitably accelerates the reduction of 4-NP. In our catalysts, the anchoring noble metal NPs on TiO_2 surface solely may increase the interface of Au and TiO_2, which will enhance the electron transfer rate between TiO_2 and Au. Additionally, the incorporation of ZrO_2 into TiO_2 restricts the grain growth of TiO_2, resulting in quite a small grain size of TiO_2, which also bestows an increased interface of Au and TiO_2. Based on the above analysis, the Fe@ZrO_2-TiO_2/Au-Pt sample exhibited enhanced catalytic activity.

Reusability is the main advantage for heterogeneous catalysts in industrial applications. In this work, magnetic Fe core was incorporated in the composite materials, which can be easily separated from the reaction media. Hence, the outflow of catalyst during the recycle process can be limited greatly. As a representative, we have investigated the reusability of the Fe@ZrO_2-TiO_2(1 : 3)/Au-Pt. As shown in Fig. S7, only a slight decrease (~18%) in the catalytic activity was observed after five successive cycles, demonstrating the remarkable stability and reusability of the Fe@ZrO_2-TiO_2(1 : 3)/Au-Pt sample.

CONCLUSIONS

We have demonstrated a facile route to selectively anchor Au-Pt alloyed NPs on the TiO_2 surface of binary ZrO_2-TiO_2 shells. The route contains the deposition of ZrO_2-TiO_2 composite oxides on ellipsoidal Fe_2O_3 NPs, modification of the composite oxides surface by Sn^{2+}, *in situ* reduction of Pt and Au, and thermal treatment to transform the Fe_2O_3 NPs to magnetic Fe NPs. Due to the unique orientation of Sn^{2+} species, the obtained Au-Pt particles were believed to be deposited on TiO_2 surface rather than on ZrO_2 surface solely. The prepared Fe@ZrO_2-TiO_2/Au-Pt catalysts showed good catalytic activity and reusability for the reduction of 4-NP. Especially, the sample that incorporation of binary oxides layer with ZrO_2 : TiO_2=1 : 3 exhibited the preferred catalytic activity and the conversion yield of 4-NP to 4-AP was still maintained at 82% even after five successive cycles. Future work will involve the varying of the binary metal oxides layers, such as TiO_2-CeO_2 or TiO_2-SiO_2, to extend the application of the strategies for selectively anchoring noble metal NPs and achieving an enhanced reactivity.

ACKNOWLEDGEMENTS

The authors are grateful to the financial support of National Natural Science Foundation of China (Grant No. 21603101, 51604155), Natural Science Foundation of Jiangsu (Grant No. BK20160774), the Introducing Talents Fund of Nanjing Institute of Technology (YKJ201505, YKJ201310), Youth Key Fund of Nanjing Institute of Technology (QKJA201401), the Opening Project

of Jiangsu Key Laboratory of Advanced Structural Materials and Application Technology (ASMA201611) and the Outstanding Scientific and Technological Innovation Team in Colleges and Universities of Jiangsu Province.

SUPPORTING INFORMATION

Additional information as noted in the text. This information is available via the Internet at http://www.springer.com/chemistry/journal/11814.

REFERENCES

1. M. Grzelczak, J. Vermant, E. M. Furst and L. M. Liz-Marzan, *Acs Nano*, **4**, 3591 (2010).
2. C. R. Lin, C. L. Yeh, S. Z. Lu, I. S. Lyubutin, S. C. Wang and I. P. Suzdalev, *Nanotechnology*, **21**, 235603 (2010).
3. M. Cargnello, M. Grzelczak, B. Rodriguez-Gonzalez, Z. Syrgiannis, K. Bakhmutsky, V. La Parola, L. M. Liz-Marzan, R. J. Gorte, M. Prato and P. Fornasiero, *J. Am. Chem. Soc.*, **134**, 11760 (2012).
4. H. Zhuang, Q. Gu, J. Long, H. Lin, H. Lin and X. Wang, *RSC Adv.*, **4**, 34315 (2014).
5. Y. Zhang, Y. Zhou, Z. Zhang, S. Xiang, X. Sheng, S. Zhou and F. Wang, *Dalton Trans.*, **43**, 1360 (2014).
6. M. M. Khan, S. Kalathil, J. Lee and M. H. Cho, *Bull. Korean Chem. Soc.*, **33**, 1753 (2012).
7. L. Delannoy, G. Thrimurthulu, P. S. Reddy, C. Methivier, J. Nelayah, B. M. Reddy, C. Ricolleau and C. Louis, *Phys. Chem. Chem. Phys.*, **16**, 26514 (2014).
8. O. A. Barias, A. Holmen and E. A. Blekkan, *J. Catal.*, **158**, 1 (1996).
9. J. Zhang, G. Chen, D. Guay, M. Chaker and D. Ma, *Nanoscale*, **6**, 2125 (2014).
10. A. Corma and P. Serna, *Science*, **313**, 332 (2006).
11. L. Zhao, N. Heinig and K. T. Leung, *Langmuir*, **29**, 927 (2013).
12. N. Liu, H. Han, Z. Yuan and Z. Ma, *RSC Adv.*, **5**, 1867 (2015).
13. J. Luo, P. N. Njoki, Y. Lin, L. Y. Wang and C. J. Zhong, *Electrochem. Commun.*, **8**, 581 (2006).
14. L. Zhao, J. P. Thomas, N. F. Heinig, M. Abd-Ellah, X. Wang and K. T. Leung, *J. Mater. Chem. C*, **2**, 2707 (2014).
15. J. Zhang, C. Hou, H. Huang, L. Zhang, Z. Jiang, G. Chen, Y. Jia, Q. Kuang, Z. Xie and L. Zheng, *Small*, **9**, 538 (2013).
16. R. Ferrando, J. Jellinek and R. L. Johnston, *Chem. Rev.*, **108**, 845 (2008).
17. L. Zhao, C. Zhang, L. Zhuo, Y. Zhang and J. Ying, *J. Am. Chem. Soc.*, **130**, 12586 (2008).
18. B. Chen, K. Lutker, S. V. Raju, J. Yan, W. Kanitpanyacharoen, J. Lei, S. Yang, H. R. Wenk, H. Mao and Q. Williams, *Science*, **338**,1448 (2012).
19. S. Panigrahi, S. Basu, S. Praharaj, S. Pande, S. Jana, A. Pal, S. K. Ghosh and T. Pal, *J. Phys. Chem. C*, **111**, 4596 (2007).
20. X. Chen, Z. Cai, X. Chen and M. Oyama, *J. Mater. Chem. A*, **2**, 5668 (2014).
21. C. Sivakumar and K. L. Phani, *Chem. Commun.*, **47**, 3535 (2011).
22. F. N. Crespilho, T. F. C. C. Borges, V. Zucolotto, E. R. Leite, F. C. Nart and O. N. Oliveira, *J. Nanosci. Nanotechnol.*, **6**, 2588 (2006).
23. Q. Zhang, D. Q. Lima, I. Lee, F. Zaera, M. F. Chi and Y. Yin, *Angew. Chem. Int. Edit.*, **50**, 7088 (2011).
24. J. Jung, S. Kang and Y. K. Han, *Nanoscale*, **4**, 4206 (2012).
25. J. Zheng, Y. Dong, W. Wang, Y. Ma, J. Hu, X. Chen and X. Chen, *Nanoscale*, **5**, 4894 (2013).
26. C. Chen, C. Nan, D. Wang, Q. Su, H. Duan, X. Liu, L. Zhang, D. Chu, W. Song, Q. Peng and Y. Li, *Angew. Chem. Int. Ed.*, **50**, 3725 (2011).
27. M. Valden, S. Pak, X. Lai and D. W. Goodman, *Catal. Lett.*, **56**, 7 (1998).
28. J. Qi, J. Chen, G. Li, S. Li, Y. Gao and Z. Tang, *Energy Environ. Sci.*, **5**, 8937 (2012).
29. W. Deng, C. Carpenter, N. Yi and M. Flytzani-Stephanopoulos, *Top Catal.*, **44**, 199 (2007).
30. X. Chen and S. S. Mao, *Chem. Rev.*, **107**, 2891 (2007).
31. B. M. Reddy and A. Khan, *Catal. Rev.*, **47**, 257 (2005).
32. H. Zou and Y. S. Lin, *Appl. Catal. A-Gen.*, **265**, 35 (2004).
33. M. E. Manriquez, M. Picquart, X. Bokhimi, T. Lopez, P. Quintana and J. M. Coronado, *J. Nanosci. Nanotechnol.*, **8**, 6623 (2008).
34. J. Liu, S. Zou, S. Li, X. Liao, Y. Hong, L. Xiao and J. Fan, *J. Mater. Chem. A*, **1**, 4038 (2013).
35. M. C. Kimling, D. Chen and R. A. Caruso, *J. Mater. Chem. A*, **3**, 3768 (2015).
36. Z. Zhang, Y. Zhou, Y. Zhang, S. Zhou, S. Xiang, X. Sheng and P. Jiang, *J. Mater. Chem. A*, **3**, 4642 (2015).
37. M. Ozaki, S. Kratohvil and E. Matijević, *J. Colloid Interface Sci.*, **102**, 146 (1984).
38. G. Yun, Z. Hassan, J. Lee, J. Kim, N. S. Lee, N. H. Kim, K. Baek, I. Hwang, C. G. Park and K. Kim, *Angew. Chem. Int. Edit.*, **53**, 6414 (2014).
39. L. Au, X. Lu and Y. Xia, *Adv. Mater.*, **20**, 2517 (2008).
40. A. P. Dementjev, A. de Graaf, M. C. M. van de Sanden, K. I. Maslakov, A. V. Naumkin and A. A. Serov, *Diam. Relat. Mater.*, **9**, 1904 (2000).
41. Y. B. He, G. R. Li, Z. L. Wang, Y. N. Ou and Y. X. Tong, *J. Phys. Chem. C*, **114**, 19175 (2010).
42. Y. Mi, J. Wang, Z. Yang, H. Wang, Z. Wang and S. Yang, *RSC Adv.*, **4**, 39743 (2014).
43. Z. Dong, X. Le, C. Dong, W. Zhang, X. Li and J. Ma, *Appl. Catal. B: Environ.*, **162**, 372 (2015).
44. X. Cui, W. Zuo, M. Tian, Z. Dong and J. Ma, *J. Mol. Catal. A: Chem.*, **423**, 386 (2016).
45. P. Zhang, C. Shao, Z. Zhang, M. Zhang, J. Mu, Z. Guo and Y. Liu, *Nanoscale*, **3**, 3357 (2011).
46. Z. D. Pozun, S. E. Rodenbusch, E. Keller, K. Tran, W. J. Tang, K. J. Stevenson and G. Henkelman, *J. Phys. Chem. C*, **117**, 7598 (2013).
47. C. M. Fan, L. F. Zhang, S. S. Wang, D. H. Wang, L. Q. Lu and A. W. Xu, *Nanoscale*, **4**, 6835 (2012).
48. W. Ye, J. Yu, Y. Zhou, D. Gao, D. Wang and D. Xue, *Appl. Catal. B: Environ.*, **181**, 371 (2016).
49. M. Tian, X. Cui, C. Dong and Z. Dong, *Appl. Surf. Sci.*, **390**, 100 (2016).
50. S. Tang, S. Vongehr and X. Meng, *J. Mater. Chem.*, **20**, 5436 (2010).
51. J. Zhang, G. Chen, D. Guay, M. Chaker and D. Ma, *Nanoscale*, **6**, 2125 (2014).
52. Z. Zhang, Y. Zhou, Y. Zhang, X. Sheng, S. Zhou and S. Xiang, *RSC Adv.*, **4**, 40078 (2014).

Supporting Information

Selective deposition of Au-Pt alloy nanoparticles on ellipsoidal zirconium titanium oxides for reduction of 4-nitrophenol

Zewu Zhang[*,,†], Jinghui Zhang[**], Guangqing Liu[***], Mengwei Xue[***], Zhangzhong Wang[*,**], Xiaohai Bu[*,**], Qiong Wu[*,**], and Xuejuan Zhao[*,**]**

*Jiangsu Key Laboratory of Advanced Structural Materials and Application Technology, Nanjing 21167, P. R. China
**School of Materials Science and Engineering, Nanjing Institute of Technology, Nanjing 21167, P. R. China
***School of Environmental Science, Nanjing Xiaozhuang University, Nanjing 21171, P. R. China
(*Received 15 December 2016 • accepted 31 May 2017*)

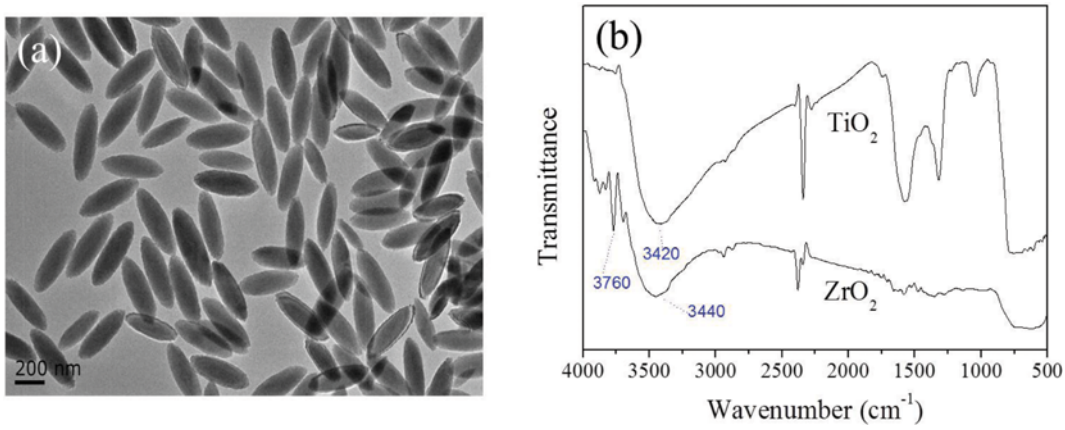

Fig. S1. (a) TEM images of the as-prepared ellipsoidal Fe_2O_3 nanoparticles, and (b) the FT-IR spectra of pure ZrO_2 or TiO_2 samples.

Fig. S2. The SEM image shows the ellipsoidal structure of the as-obtained Fe_2O_3/ZrO_2-TiO_2(1 : 1)/Au-Pt NPs.

REFERENCES

1. Z. Wang, H. Fu, D. Han and F. Gu, *J. Mater. Chem. A*, **2**, 20374 (2014).
2. Y. H. Deng, Y. Cai, Z. K. Sun, J. Liu, C. Liu, J. Wei, W. Li, C. Liu, Y. Wang and D. Y. Zhao, *J. Am. Chem. Soc.*, **132**, 8466 (2010).
3. C. M. Fan, L. F. Zhang, S. S. Wang, D. H. Wang, L. Q. Lu and A. W. Xu, *Nanoscale*, **4**, 6835 (2012).
4. P. Zhang, R. Li, Y. M. Huang and Q. W. Chen, *Acs Appl. Mater. Inter.*, **6**, 2670 (2014).
5. A. J. Ma, J. Xu, X. H. Zhang, B. Zhang, D. Y. Wang and H. L. Xu, *Sci Rep-Uk*, **4**, 4849 (2014).
6. Z. Zhang, Y. Zhou, Y. Zhang, S. Zhou, S. Xiang, X. Sheng and P. Jiang, *J. Mater. Chem. A*, **3**, 4642 (2015).

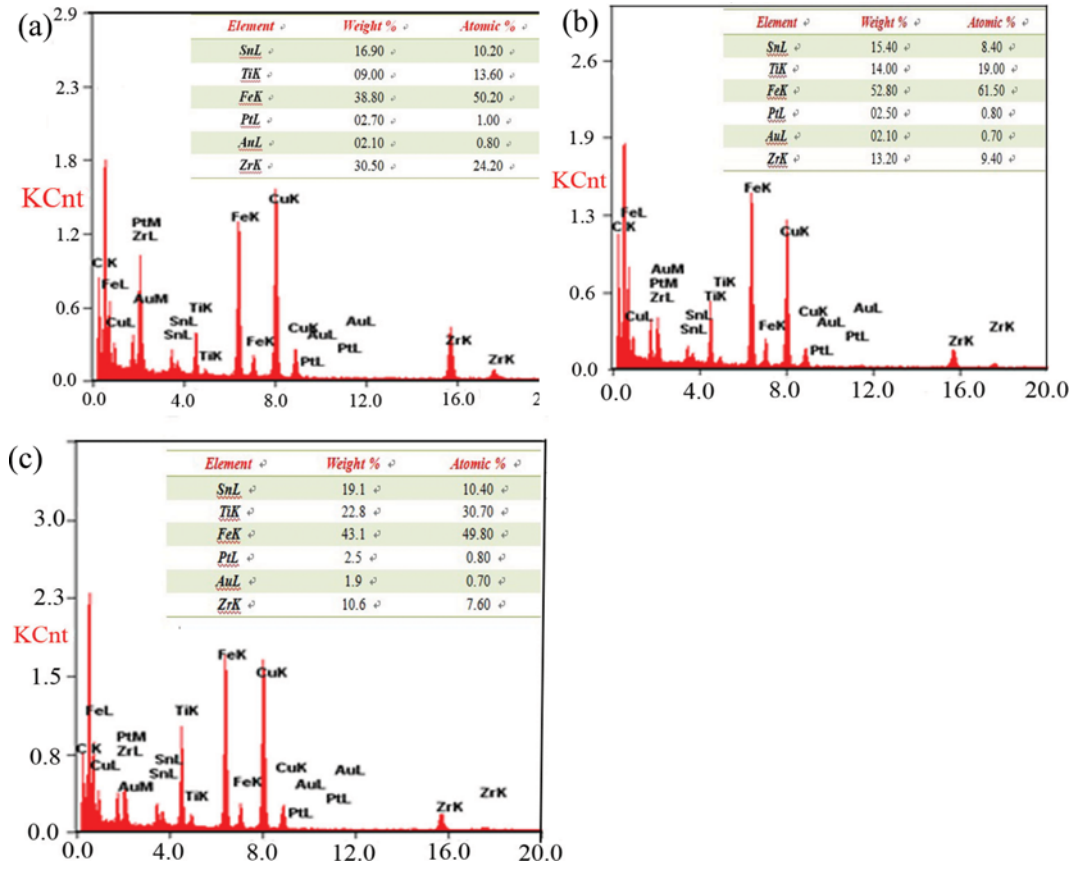

Fig. S3. The EDX spectra of the as-obtained Fe_2O_3/ZrO_2-TiO_2(x : y)/Au-Pt and the corresponding element content (inset). x : y=3 : 1 (a), 1 : 1 (b), and 1 : 3 (c).

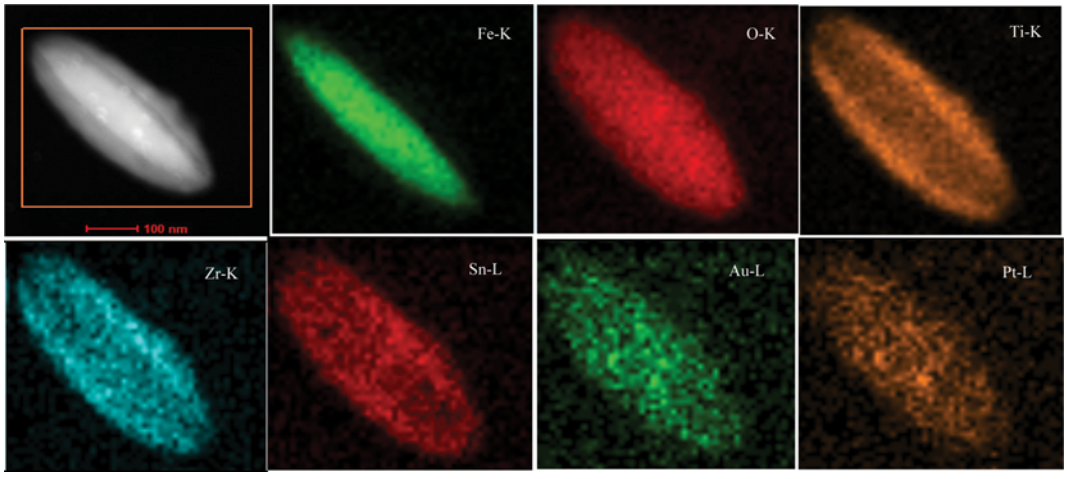

Fig. S4. HAADF-STEM image of the as-obtained Fe_2O_3/ZrO_2-TiO_2(3 : 1)/Au-Pt, Fe mapping image (Fe-K), O mapping image (O-K), Ti mapping image (Ti-K), Zr mapping image (Zr-K), Sn mapping image (Sn-L), Au mapping image (Au-L) and Pt mapping image (Pt-L) (The Si mapping image was not shown).

Table S1. Comparison of rate constant for the catalytic reduction of 4-NP by $NaBH_4$ using catalysts containing Au and (or) Pt nanoparticles

Catalyst	Size of noble metal NPs (nm)	Initial concentration of 4-NP (mM)	Amount of noble NPs (nmol)	k_{app} per noble NPs content (10^{-2} $s^{-1}\mu mol^{-1}$)
$Au@SiO_2$ [1]	40	0.1	135.9	1.40
$Fe_3O_4@SiO_2$-Au@m-SiO_2 [2]	12	0.24	335	1.74
Au-CeO_2 [3]	4	0.068	4.55	281
Fe_3O_4/C/Pt-Pd [4]	10-20	0.05	1.68	1202
Au-Pt-Ag [5]	2.2	0.083	2.5	1470
$Fe@SiO_2$/Au-Pt [6]	10	0.37	1.989	1392
$Fe@ZrO_2$-TiO_2(1 : 3)/Au-Pt (This work)	7.8	0.37	1.989	2237

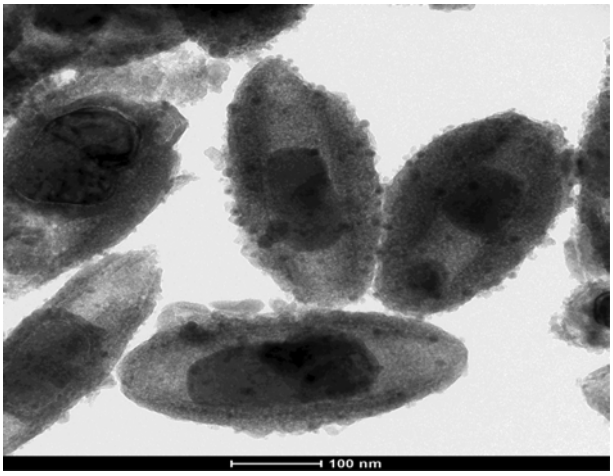

Fig. S5. The representative TEM images of $Fe@ZrO_2$-TiO_2(1 : 3)/Au-Pt NPs.

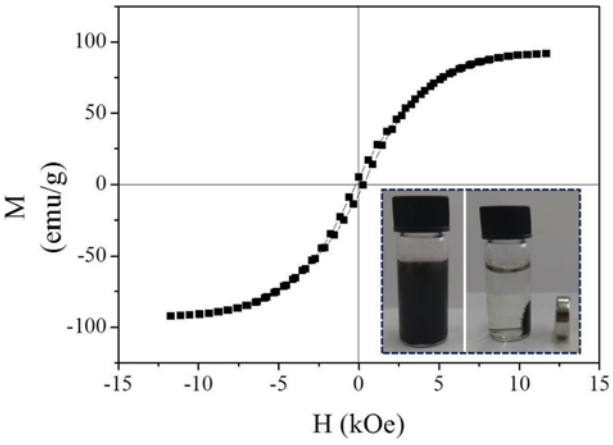

Fig. S6. Magnetization curves of the $Fe@ZrO_2$-TiO_2/Au-Pt NCs. The inset pattern is a photograph of the magnetic separation.

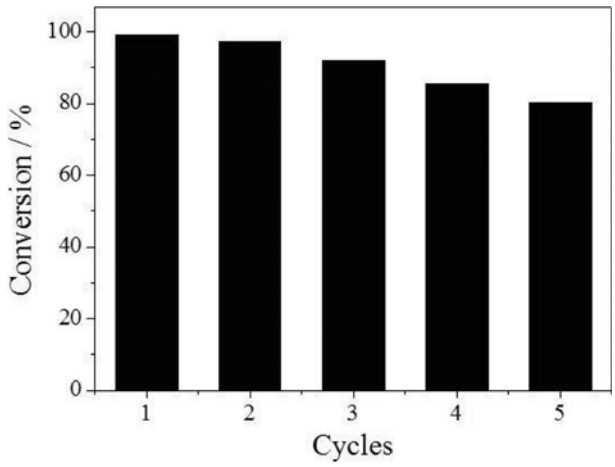

Fig. S7. Conversion of 4-NP in 5 successive cycles of reduction using $Fe@ZrO_2$-TiO_2(1 : 3)/Au-Pt NPs as catalyst.